© 2022. Paweł Szklennik.   **pp. 289 –305**

Research paper

Numerical determination of load of a model tunnel lining, taking into account different heights of soil backfill

Paweł Szklennik[1]

Abstract: The paper presents an analysis of determining the load of a model tunnel lining in a non-cohesive soil medium at two different heights of soil backfill above the structure. A series of simulations were performed with the flexible and rigid tunnel lining. The analysis was performed by conducting simulations with the use of an author's program based on the discrete element method. The model previously calibrated on the basis of laboratory tests was used. The loads acting on the structure, the distribution of stresses in the surrounding soil medium and the displacements of this medium in the vicinity of the structure were determined and compared. The effect of soil weight and technological load applied from the surface was taken into account. The values of the numerically obtained loads of the tunnel lining were compared with those calculated according to the classic Hewett's method.

It has been proven that in both cases the degree of cooperation between the structure and soil is significantly related to the rigidity of the structure, hence the loads determined may differ significantly from the results obtained according to classical methods. It was shown that discrete modelling allows to reflect differences in the behaviour of the soil medium resulting from different heights of soil backfill. Smaller horizontal pressure was obtained in the side zones of an excavation at a higher backfill. In addition, significantly greater intensity of vertical soil displacements over the lining were observed with a lower backfill height.

Keywords: discrete element method, cylindrical tunnel lining, underground tunnel

[1]PhD., Eng., Military University of Technology, Faculty of Civil Engineering and Geodesy, ul. Gen. Sylwestra Kaliskiego 2 00-908 Warsaw, Poland, e-mail: pawel.szklennik@wat.edu.pl, ORCID: 0000-0001-9383-858X

1. Introduction

The performance of a tunnel excavation in the soil medium causes a change in the original system of the principal stress trajectories. The changed trajectory system influences the transmission of loads to the excavation lining. In the literature, various proposals considering this phenomenon can be found. The Hewett's method is most popular in the case of rigid linings [1]. It is assumed here that loads are transferred to the lining as shown in Fig. 1 – the vertical load q_{v1} results from a backfill weight and possible external surface loads, the vertical reaction q_{v2} additionally includes own weight of the lining structure, the horizontal pressure q_h is dependent on the soil lateral pressure coefficient.
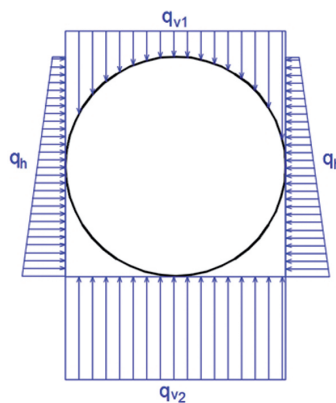

Fig. 1. The system of actions on the cylindrical tunnel lining
according to Hewett's proposal

This load scheme is an idealization that does not take into account the so-called "arching effect" resulting in a new principal stress trajectory and a change in the distribution of actions on the lining. Another of the existing methods proposed by Bodrow and Gorelik [2, 3] is appropriate for deep tunneling. To this should be added mining methods – the design of permanent linings in mines is regulated by the standard [4]. When determining the loads, the methods proposed by Protodiakonow, Bierbaumer, Cymbariewicz, Terzaghi, Sałustowicz [5] taking into account the effects of arching effect in various ways were adopted there.

In the case of linings with low rigidity, the need to take into account the effect of deformation of the lining structure becomes of particular importance. It causes passive pressure and a change in the stress trajectory in the side areas, which increases the load on this part of the structure. This effect is sometimes taken into account in design procedures by introducing a coefficient that increases the horizontal pressure, but without reducing the vertical pressure at the same time. More precise proposals for describing these phenomena were included in the works of Pytowski [6] and Spangler [7]. In both studies, only the deformation effects of bending with neglect of longitudinal forces were taken into account, such a state can be described as causing regular flattening of the load–bearing structure.

In most of the above–mentioned methods, deformation of the lining is determined for loads assumed a priori, and not determined as a result of its interaction with the soil. Moreover, the friction forces caused by deformations of the soil medium adjacent to the structure as well as imperfections in the zone of contact of the structure with the soil and in the soil itself are neglected.

The above–mentioned limitations can be eliminated using numerical methods. In the case of continuous models, e.g. according to the finite element method or the finite difference method, discretization of the medium does not change the basic assumption about the continuity of the medium, it only partially reduces it. This approach may correspond to cohesive soils with a compact structure. In the case of non-cohesive granular soils, the results of the analyzes are subject to some error here. The actual soil medium deformation mechanisms, characterized by mutual displacements of grains while overcoming frictional resistance and not deformation of single grains, are neglected. Reliable results might be expected here using so-called discrete methods [8, 9]. They describe the medium as a set of individual elements, interacting with forces determined in accordance with the assumed constitutive model of contact. In addition, such a numerical soil model is characterized by a certain degree of geometric irregularities, and therefore takes into account local imperfections – voids between soil grains, which are additionally subject to evolution in the process of deformation.

The purpose of this study is to verify an adequacy of the novel approach to the analysis of loads acting on the model lining of a tunnel excavation in non-cohesive soil, considering different heights of soil backfill above the tunnel and different flexibility of the lining. It was tested if the discrete modelling allows to reflect effects neglected in the aforementioned theoretical methods. Additionally, the stresses and displacements of the soil in the lining surroundings were determined. The results presented in [10] were compared with the results obtained with greater backfill height above the construction. The analyzes were conducted with the use of the author's program based on the Discrete Element Method (DEM) [11].

2. Discrete element method (DEM)

The discrete element method is mainly used to analyze dynamics problems [12, 13]. Simulations of direct shear [9, 14] or triaxial compression [8] can be mentioned among the application of this method to the testing of a granular medium. It is also used for modelling rocks, [15, 16] or concrete [17, 18]. The disadvantage of discrete methods is the high computational cost of simulating more complex issues, resulting from the required number of elements, which is particularly important in the case of simulations in a loose medium, where the list of contact pairs of elements is changing and therefore requires constant updating. On the other hand, continuous methods present some difficulties in direct modelling of a granular medium containing irregularities and discontinuities undergoing grain rearrangements. These are the main reasons why it is proposed to combine continuous and discrete modelling, such as FEM and DEM, in one simulation [19–21]. Solid materials are then modelled with FEM and interacting granular medium is described with DEM, assuming their adequate mutual contact model.

The essence and detailed description of the discrete element method used in the analyzes, including the characteristics and physical meaning of the parameters of the discrete model, are presented in [11,21]. The idea of this method is to model the medium directly as a set of individual elements of a specific shape that can interact with each other by contact forces calculated in accordance with the assumed constitutive model of local contact. This model must correspond to the properties of a given material. In addition to the normal force, the contact may include, among others, friction and damping. The elastic brittle model is relatively simple. The more complex variants include, for example: models with a gradual decrease in bond stiffness, elasto–plastic and elasto–plastic softening models. Depending on the material to be described, the contact may be a bond working on the forces of both signs or only on compression. Spherical (3D) and cylindrical (2D)–shaped particles are often used, which is related to the much more difficult determination of the mutual contact of elements with irregular shapes. Elliptical elements or cluster elements made of interpenetrating or "stuck together" spheres or cylinders are also used. The main operations performed during the calculations are: searching for pairs of elements in contact, calculating contact interactions between them, updating the position of elements on the basis of equations of motion.

A typical constitutive model of the contact of elements, also used in this paper, is shown in Fig. 2. It is described by the stiffness modulus for the normal direction (k_n) and tangential direction (k_s), the damping coefficient c_n and sliding friction coefficient μ. The program used also allows taking into account the rolling friction and external damping.
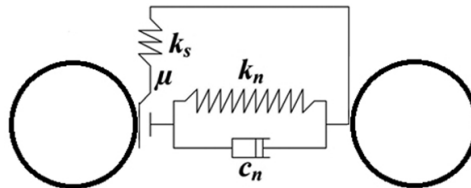

Fig. 2. Model of the contact of two discrete elements

By dividing the normal force into the elastic and damping part, it can be written:

$$F_n = F_n^e + F_n^d$$

The elastic part is designated as:

$$F_n^e = k_n \cdot g_n$$

where: g_n – the mutual "overlapping" of the elements at a given moment.

The damping part, on the other hand, is determined for the viscous damping according to the relationship:

$$F_n^d = c_n \cdot v_n$$

where: v_n – normal component of the relative velocity at the point of contact between the elements.

The damping is conveniently related to the critical damping value c_{cr} using a factor α_c according to the relation:

$$c_n = \alpha_c \cdot c_{cr}$$

The tangential force in the absence of cohesion is determined according to the regularized Coulomb friction law presented in Fig. 3. The maximum possible value of the friction force is therefore:

$$F_s^{\max} = \mu \, |F_n|$$
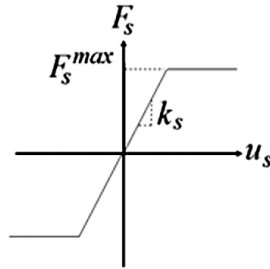
Fig. 3. Regularized Coulomb friction law
introduced in DEM [20]

The value of the tangential force in a given local contact is updated in every time step n on the basis of the value of the so-called incremental slip Δu_s and the tangential stiffness according to the relationship:

$$F_s^{\text{test}} = F_s^{n-1} + k_s \cdot \Delta u_s$$

where: F_s^{test} – so-called test value of the tangential force.

Another effect is the rolling friction resistance M_f determined on the basis of the relative rotational speed $\dot{\Phi}_r$ at the point of contact, the assumed "rolling resistance stiffness" k_θ and the rolling friction coefficient f in a manner analogous to determining the sliding friction resistance. The maximum possible rolling resistance value will therefore be $M_f^{\max} = f \, |F_n|$.

In order to carry out a numerical simulation, the simulation time assumed at the beginning of the calculations is divided into time steps Δt. At each time step, linear and rotational accelerations are determined for each element according to the Newton's equations of motion. The equations of motion are integrated using an explicit or implicit scheme in order to determine the velocity and displacements.

3. Author's DEM program

The previously described so-called "soft" contact model was applied in the author's program for determining the normal contact force. It is presented in [11], it assumes a linear relationship between the stiffness of the element and its size. Elastic contact in the normal

direction between two particles is considered as for two elements of a certain stiffness positioned in series. The stiffness of the i element is therefore:

$$k_{n,i} = \frac{E_i A_i}{d_i}$$

where: E_i is the material's modulus of elasticity, d_i is the assumed length of the hypothetical elastic element corresponding to the particle i, A_i is the area of its "cross-section". Finally, the local stiffness of the contact of two given discrete elements no. 1 and 2 is as follows:

$$k_n = \frac{k_{n,1} \cdot k_{n,2}}{k_{n,1} + k_{n,2}}$$

The tangential force, sliding and rolling friction are also taken into account in the simulation. In order to determine the stiffness of sliding and rolling friction, the approach presented, among others, in [8] was applied. The stiffness in the tangential direction was taken as

$$k_s = k_n \nu^c$$

where: ν^c – so-called Poisson's ratio for local contact.

Rolling resistance stiffness is

$$k_\theta = \beta k_s r_1 r_2$$

where: β – proportionality factor, r_1 and r_2 – the radii of the elements in contact.

The rolling friction coefficient f was determined by the multiplier ε according to

$$f = \varepsilon r_a$$

where: r_a – the average radius length of the two contacting elements.

The ability to determine averaged stresses at any point in the modeled medium was implemented in the computer program. It is the issue of homogenization and averaging [22–24] consisting in determining certain quantities in the macro scale based on the known results in the micro scale – in this case at the level of the individual discrete elements. The applied method is based on the concept of the representative volumetric element (RVE) [25, 26]. For any point of the modeled medium, the surrounding area is determined – the RVE volume – in which the sought value will be averaged. The RVE size should be large enough to avoid micro–scale fluctuations, but also not too large for the calculated values to be treated as local.

A more detailed description of the author's numerical program is provided in [10, 27].

4. Numerical model of the tunnel lining

Numerical analysis was carried out on the submerged in soil model lining of the cylindrical excavation (Fig. 4). Due to the limitations of the computing capabilities of the computer and the laboratory stand, the scaled model was tested. The width of the

soil medium area along the X axis is 80 cm, the lining recessed in it has a diameter of $d = 90$ mm. The soil was modeled with cylindrical elements as a system in a plane stress state. The lining was made of cylindrical elements connected by bonds with a stiffness specific to HDPE (a variant of the flexible structure) or infinitely high stiffness (a rigid structure). The boundary conditions of the model corresponded to the stand used for its calibration during laboratory tests – flat rigid planes were placed at the left, right and bottom edge of the analyzed area, while free top edge was subjected to external sectional load Q. The resultant Q value was 1250 N and it was evenly distributed over a length of 45 cm, symmetrically with respect to vertical axis of the excavation.
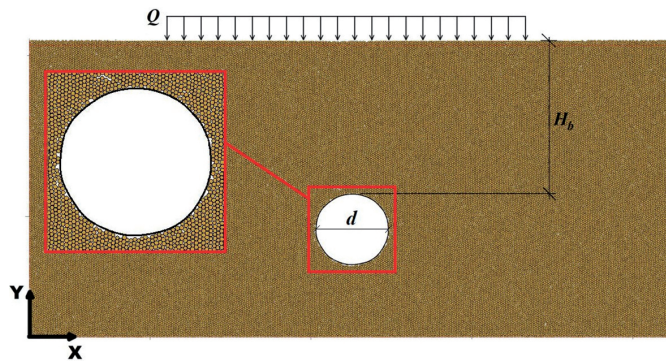

Fig. 4. DEM model used in numerical analyzes

Models with soil backfill height equal to the diameter of the lining ($H_b = d$, denoted as H_{b1}) and equal to two diameters ($H_b = 2d$, denoted as H_{b2}) were considered – Fig. 4. The diameters of soil elements were assumed to be $\Phi_{el}^{DEM} = 2 \div 2.5$ mm, randomly distributed. The number of discrete elements modeling soil was 43756 for the H_{b1} model and 58341 for the H_{b2} model. An explicit scheme for integration of equilibrium equations over time was used in the DEM procedure. The time step in the simulation was equal to $\Delta t = 5.5 \cdot 10^{-7}$ s.

The calibration process of the presented model, carried out on the basis of comparing the lining deformation in the simulation with the deformation in the laboratory model, is described in [27]. The list of determined material parameters and parameters of contact of elements together with their designations are given in Tables 1 and 2. The symbols used in the subscript denote a given material or pairs of surfaces to which they relate.

Table 1. Material parameters of the numerical model

Material parameter	Material	
	Soil medium (gravel)	lining (HDPE)
Young modulus	$E_s = 9$ MPa	$E_t = 500$ MPa
Specific density	$\rho_s = 2550 \ \dfrac{\text{kg}}{\text{m}^3}$	$\rho_t = 10000 \ \dfrac{\text{kg}}{\text{m}^3}$

Table 2. Parameters of contact in the numerical model

Parameters of contact	Type of contact			
	soil–soil	lining–lining	lining–soil	edge–soil
Poisson's ratio	$v_s^c = 0.15$	$v_t^c = 0.45$	$v_{t-s}^c = 0.3$	$v_{e-s}^c = 0.15$
Proportionality factor for determining the stiffness of the rolling resistance	$\beta_s = 50$	absent	$\beta_{t-s} = 50$	$\beta_{e-s} = 50$
Sliding friction coefficient	$\mu_s = 0.25$	absent	$\mu_{t-s} = 0.1$	$\mu_{e-s} = 0.1$
Parameter for determining the rolling friction coefficient	$\varepsilon_s = 0.4$	absent	$\varepsilon_{t-s} = 0.1$	$\varepsilon_{e-s} = 0.1$
Viscous damping factor	$\alpha_{c,s} = 0.5$	absent	$\alpha_{c,t-s} = 0.5$	$\alpha_{c,e-s} = 0.5$

The calibrated model was then used to perform the analyzes presented later in this work in order to determine the loads on the lining. Also the maps of stresses and displacements in the soil medium were created by determining them at grid points (Fig. 5). To calculate the average stresses, the optimal RVE diameter was determined to be 1 cm. The resulting stresses are only compressive (non-cohesive medium).
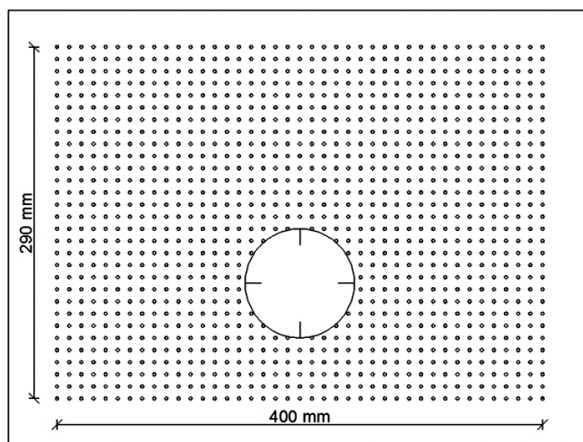

Fig. 5. Arrangement of measuring points for determining the averaged stresses
in the medium and displacements of elements

Actions on the structure were defined as averaged sectional loads projected on the vertical and horizontal directions in the global XY system (denoted as L, P, G, D), as well as on individual sections of the chord of the lining (denoted as W1–W8). The location and length of the sections are shown in Fig. 6.
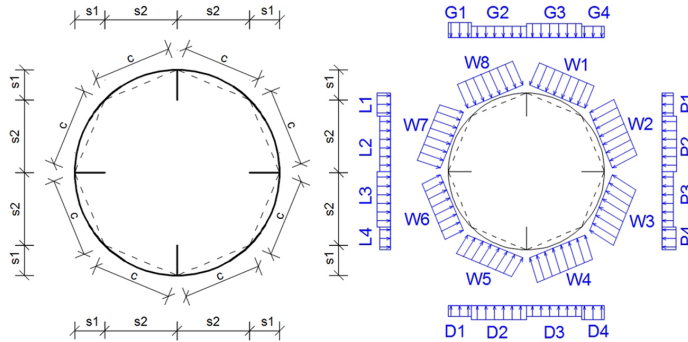
Fig. 6. Denotings of the lengths of sections and loads

5. Analysis of the results

The chapter presents the values of the loads transferred to the lining obtained in DEM simulations compared to the actions determined according to the Hewett's method. Also the maps of stresses and displacements in the soil medium are presented. There are abbreviated model designations for the rigid tunnel lining structure (RT) or flexible tunnel lining structure (FT).

The values of the vertical and horizontal Hewett loads are presented in Fig. 7. Analogous values obtained by the DEM for the flexible lining (Fig. 8) indicate a reduction in vertical interactions in the crown area of the lining and an increase in horizontal interactions in the side areas. This phenomenon is more intense at lower soil backfill (H_{b1}) – there is about 10% greater horizontal pressure than in the H_{b2} model.
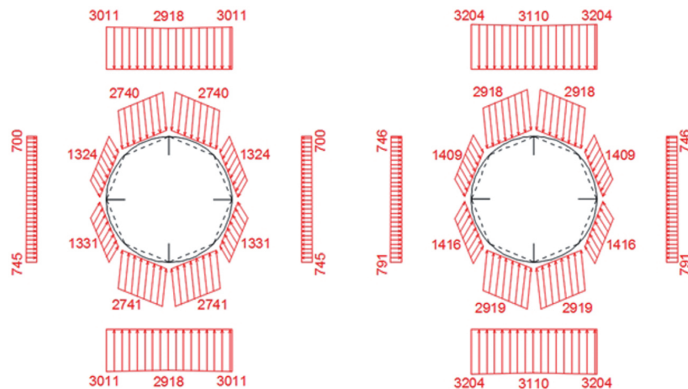
Fig. 7. Actions according to Hewett's method [N/m] – H_{b1} (left) and H_{b2} (right) models

In the case of the rigid structure (Fig. 9), the vertical actions are largely consistent with the Hewett's method. However, there is a clear reduction of horizontal forces here, which results from the lack of passive pressure in the side area.
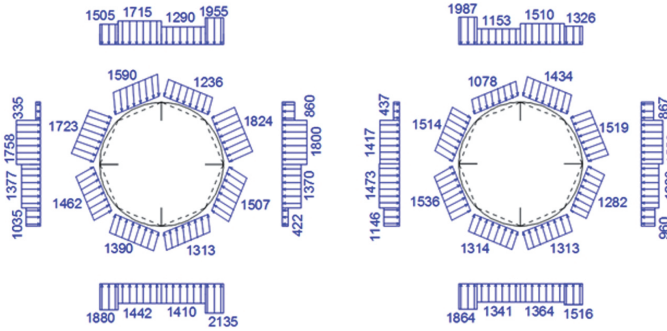
Fig. 8. Actions according to DEM [N/m] – H_{b1} (left) and H_{b2} (right) models,
flexible tunnel lining (FT)
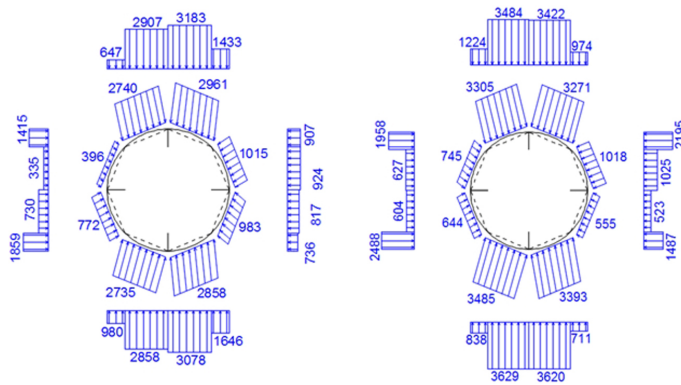
Fig. 9. Actions according to DEM [N/m] – H_{b1} (left) and H_{b2} (right) models,
rigid tunnel lining (RT)

Comparative diagrams of the loads on the flexible (FT) and rigid (RT) tunnel linings according to DEM and the Hewett's method are shown in Figs. 10 and 11. Generally, the Hewett's method regardless of the stiffness of the structure, gives lower values of the total sectional loads L2, L3 and P2, P3.
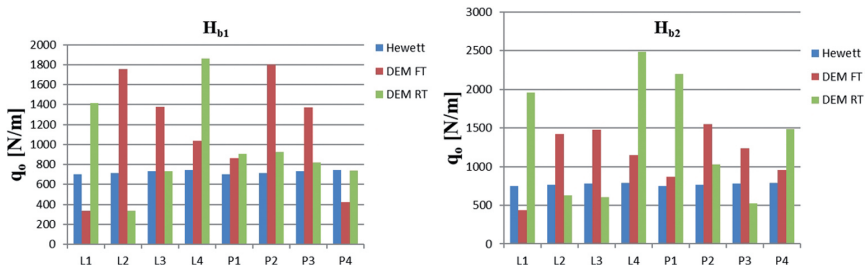
Fig. 10. Horizontal actions on the lining – H_{b1} and H_{b2} models
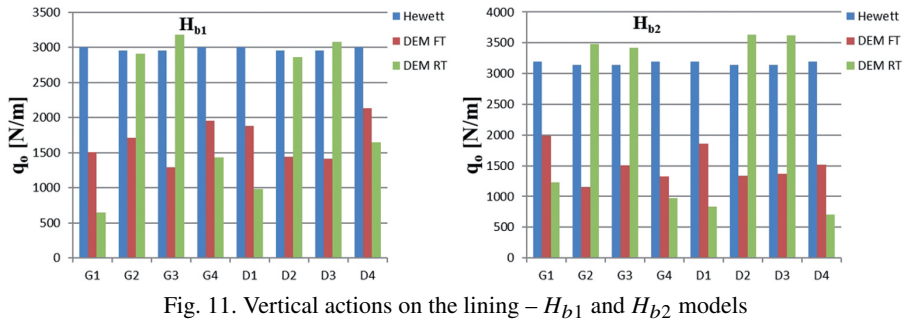
Fig. 11. Vertical actions on the lining – H_{b1} and H_{b2} models

The lining flexibility reduces the vertical loads transferred to its crown part – G2, G3 loads and D2, D3 reactions (Fig. 11). The same sectional actions for the rigid lining and according to Hewett can be considered consistent.

These observations correspond with the maps of horizontal stresses in the case of flexible lining for both H_{b1} and H_{b2} variants (Fig. 12). There are significant concentrations at the side sections of the lining, reaching 18 kPa. In the case of the rigid structure (Fig. 13), they do not exceed 8÷10 kPa.
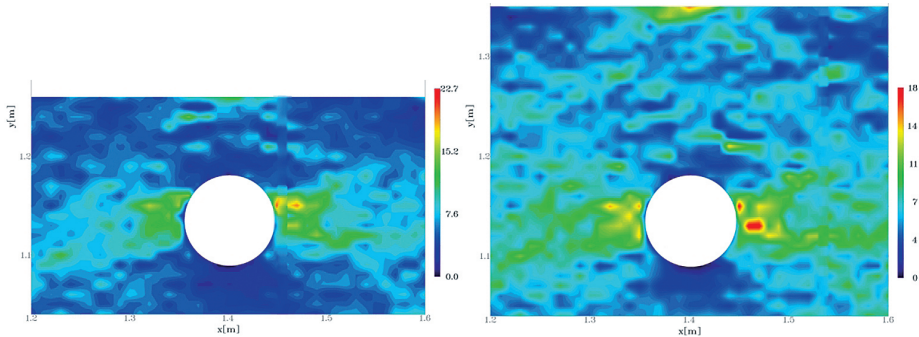
Fig. 12. Map of horizontal stresses σ_x [kPa] – H_{b1} and H_{b2} models, flexible tunnel lining (FT)
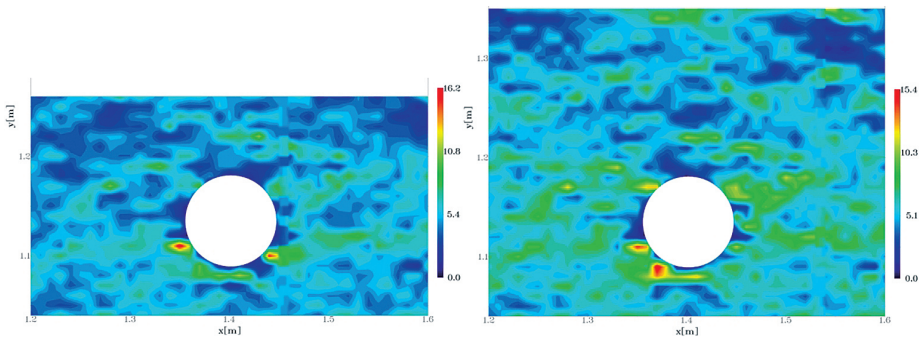
Fig. 13. Map of horizontal stresses σ_x [kPa] – H_{b1} and H_{b2} models, rigid tunnel lining (RT)

The vertical stress maps for the flexible lining (Fig. 14) in the case of both backfill heights show the stress concentration in the areas directly adjacent to the side of the structure. This observation is qualitatively consistent also for the rigid lining (Fig. 15). These stresses in both cases reach the order of 40 kPa, which is over 200% of the stresses caused at the same depth in the area remote from the excavation. The deformation of the flexible structure significantly reduces the vertical stresses over the excavation, which is closely related to the reduction of loads on the structure itself in this direction. This phenomenon does not occur with a rigid lining – σ_y in the crown part are of the order of 30 kPa, while above the flexible lining they are approx. 12 kPa. Similar values of stresses occur under the invert section.
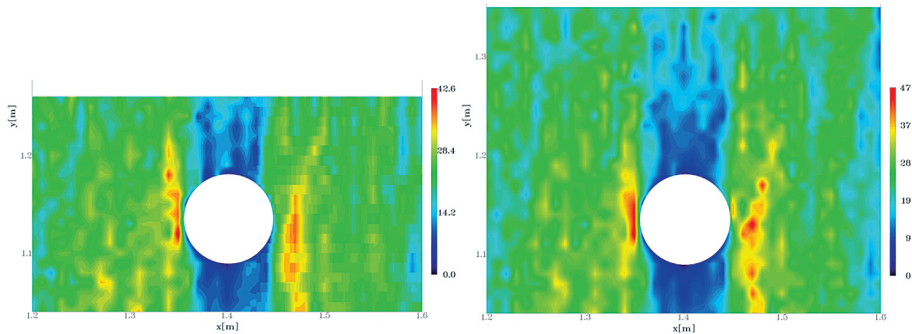
Fig. 14. Map of vertical stresses σ_y [kPa] – H_{b1} and H_{b2} models, flexible tunnel lining (FT)
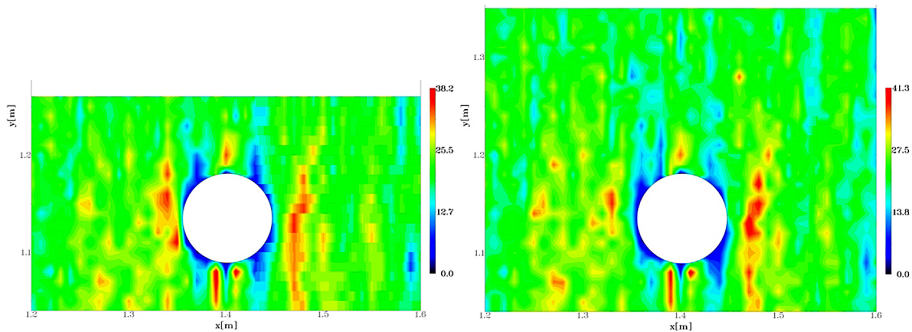

Fig. 15. Map of vertical stresses σ_y [kPa] – H_{b1} and H_{b2} models, rigid tunnel lining (RT)

When analyzing the maps of horizontal displacements of the soil (Δx) in the surroundings of the side parts of the excavation (Figs. 16, 17), their relatively low values are found in the vicinity of the rigid lining (approx. 0.3 mm). The natural concentration of these displacements is visible in the case of the flexible structure. Here they amount to 0.7–0.9 mm, their form is qualitatively consistent at both backfill heights. The maps of vertical displacements of the soil (Δy) show different intensities of its subsidence (Figs. 18, 19). In the case of the flexible lining, the strong displacement concentration caused by deformations

of the structure's crown part is visible. The area of subsidence over the rigid lining is characterized by considerable extension and lower intensity. From these maps it is possible to conclude on the influence of the height of the soil backfill on the way of transferring technological loads to the flexible lining. This difference manifests itself in significantly greater displacements of the soil over the excavation at a lower backfill height H_{b1} (Fig. 18).
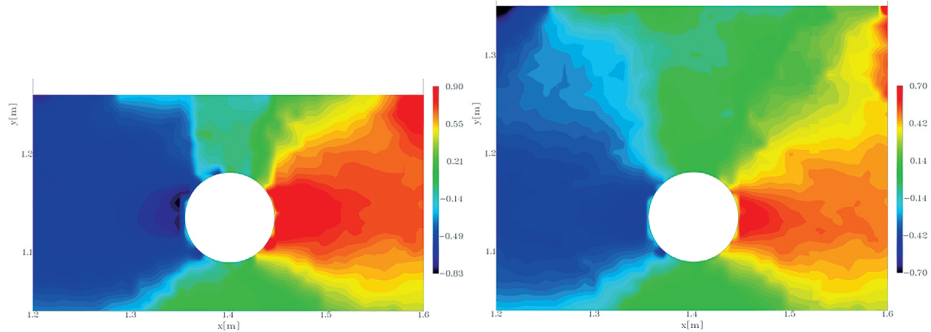

Fig. 16. Map of horizontal displacements Δ_x [mm] – H_{b1} and H_{b2} model, flexible tunnel lining (FT)
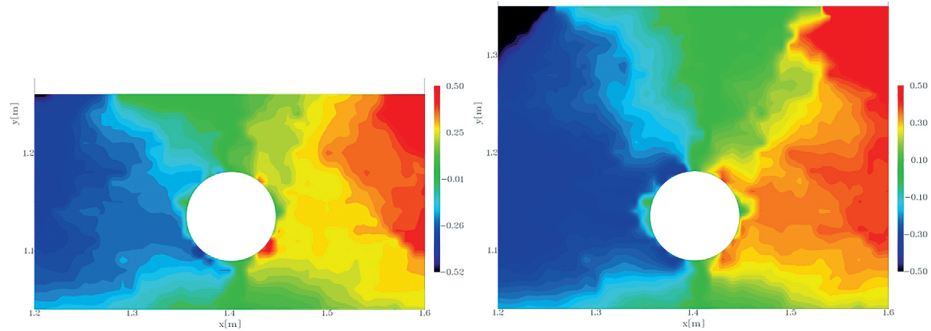

Fig. 17. Map of horizontal displacements Δ_x [mm] – H_{b1} and H_{b2} model, rigid tunnel lining (RT)
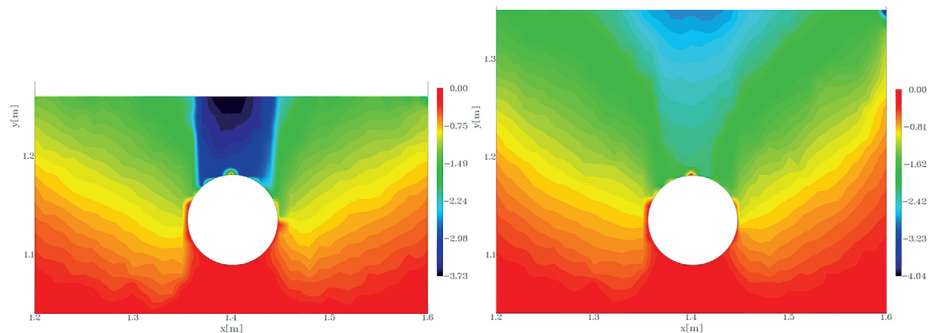

Fig. 18. Map of vertical displacements Δ_y [mm] – H_{b1} and H_{b2} model, flexible tunnel lining (FT)

Qualitatively different forms of the subsidence basin in the ground surface level are also obtained in the case of the rigid structure (Fig. 19). It is more extensive in the H_{b2} model than in the H_{b1} model, where its area is concentrated in the strip above the excavation.
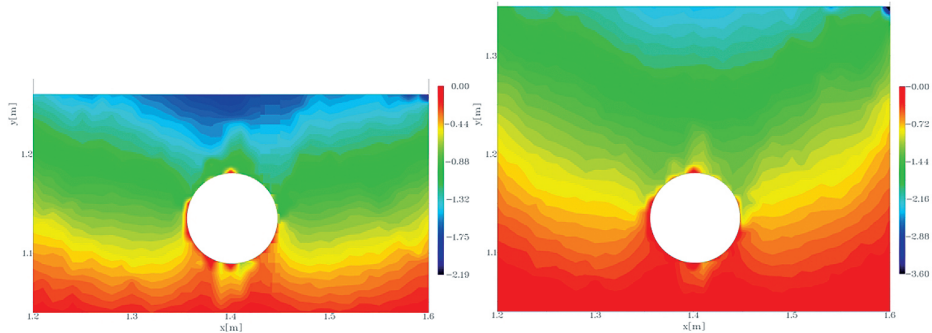

Fig. 19. Map of vertical displacements Δ_y [mm] – H_{b1} and H_{b2} model, rigid tunnel lining (RT)

6. Summary

It has been shown that the value of loads acting on the model tunnel lining is significantly influenced by its deformation and arching effect in the surrounding soil. The arching effectiveness is clearly visible already in the case of the backfill height equal to one diameter of the lining and is present also at its greater height. In the case of the flexible lining, the vertical actions transferred to its crown part are reduced. At the same time, vertical stresses in the soil increase in the side area of the excavation, which significantly intensifies the lateral pressure on the lining. Comparing these results with typical load schemes in design procedures, it can be seen that these schemes may not include the most unfavorable load situation. The differences may concern both the side and crown zones and are clearly visible for lower and higher backfill.

The adequacy of discrete modeling is also supported by the fact that it allows to reflect the influence of the height of the backfill on the intensity of the load acting on the lining and the distribution of stresses and displacements in its surroundings. For example, smaller horizontal pressure was obtained in the side zones of the flexible lining at a higher backfill. Also in the case of soil displacements, significant differences in the intensity of subsidence are shown – it is definitely higher with lower backfill height. The discrete model also captures non-stationary imperfections in the soil medium, visible in a certain asymmetry of the resulting interaction forces. When applying DEM, it is taken into account that the soil has an internal skeleton that interacts with the tunnel lining. The inward deformation of the lining structure causes its relief, while the reverse deformations cause passive resistance in the soil, increasing the total pressure in a given section.

The above–mentioned results confirm that the presented numerical approach is effective in tunnel loads determination. It should be noted that the soil conditions in the presented

analyzes were relatively simple, and the scale effect was not considered. Therefore, for the final assessment of the extent to which presented analyses can be adapted to a tunnel and the DEM capabilities in this regard, it is necessary to identify the model on a 1:1 scale using reliable data on the real structure.

References

[1] B.H.M. Hewett, S. Johanneson, *Schild und Druckluft Tunnelbau*. Düsseldorf: Werner Verlag, 1964.

[2] H. Stamatello, *Tunele i miejskie budowle podziemne*. Warszawa: Arkady, 1970.

[3] S.S. Dawydow, *Obliczanie i projektowanie konstrukcji podziemnych*. Warszawa: MON, 1954.

[4] *PN-G-05020:1997 – Podziemne wyrobiska korytarzowe i komorowe – Obudowa sklepiona – Zasady projektowania i obliczeń statycznych*.

[5] E. Świst, *Hydrotechniczne i komunikacyjne budowle podziemne*. Bielsko–Biała: Wydawnictwo STO,2006.

[6] J. Bartoszewski, S. Lessaer, *Tunele i przejścia podziemne w miastach*. Warszawa: Wydawnictwa Komunikacji i Łączności, 1971.

[7] R.W. Abbett, *American Civil Engineering Practice*. New York: John Wiley & Sons, Inc., 1956.

[8] Ł. Widuliński, J. Kozicki, J. Tejchman, "Numerical Simulations of Triaxial Test with Sand Using DEM", *Archives of Hydro-Engineering and Environmental Mechanics*, 2009, vol. 56, no. 3–4, pp. 149–172.

[9] Y. Yan, S. Ji, "Discrete element modeling of direct shear tests for a granular material", *International Journal for Numerical and Analytical Methods in Geomechanics*, 2010, vol. 34, no. 9, pp. 978–990, DOI: 10.1002/nag.848.

[10] P. Szklennik, „Analiza numeryczna interakcji modelowej obudowy tunelowej z gruntem niespoistym", *Biuletyn WAT*, 2019, vol. 68, no. 1, pp. 175–195, DOI: 10.5604/01.3001.0013.1479.

[11] P.A. Cundall, O.D.L. Strack, "A discrete numerical model for granular assemblies", *Géotechnique*, 1979, vol. 29, no. 1, pp. 47–65, DOI: 10.1680/geot.1979.29.1.47.

[12] F. Bourrier, F. Nicot, F. Darve, "Evolution of the micromechanical properties of impacted granular materials", *Comptes Rendus Mecanique*, 2010, vol. 338, no. 10–11, pp. 639–647, DOI: 10.1016/j.crme.2010.09.007.

[13] L. Wu, T. Guan, "Discrete element model for analysis of chamber pressure of earth pressure balance shield machine" in *Proceedings of 2010 International Conference on Mechanic Automation and Control Engineering (MACE), Wuhan*. 2010, pp. 671–674, DOI: 10.1109/MACE.2010.5535730.

[14] P. Szklennik, "Numeryczne analizy bezpośredniego ścinania gruntu niespoistego z zastosowaniem metody elementów dyskretnych", *Budownictwo i Inżynieria Środowiska*, 2012, vol. 3, no. 4, pp. 211–216.

[15] Y. Wang, F. Tonon, "Calibration of a discrete element model for intact rock up to its peak strength", *Int. J. Numerical and Analytical Methods in Geomechanics*, 2010, vol. 34, no. 5, pp. 447–469, DOI: 10.1002/nag.811.

[16] C. Müller, T. Frühwirt, D. Haase, R. Schlegel, H. Konietzky, "Modeling deformation and damage of rock salt using the discrete element method", *International Journal of Rock Mechanics and Mining Sciences*, 2018, vol. 103, pp. 230–241, DOI: 10.1016/j.ijrmms.2018.01.022.

[17] S. Hentz, L. Daudeville, F.V. Donzé, "Identification and validation of a discrete element model for concrete", *ASCE Journal of Engineering Mechanics*, 2004, vol. 130, no. 6, pp. 709–719, DOI: 10.1061/(ASCE)0733-9399(2004)130:6(709).

[18] B. Beckmann, K. Schicktanz, M. Curbach, "Discrete Element simulation of concrete fracture and crack evolution", *Beton und Stahlbetonbau*, 2018, vol. 113, pp. 91–95, DOI: 10.1002/best.201800045.

[19] K. Han, D. Peric, A.J.L. Crook, D.R.J. Owen, "A combined finite/discrete element simulation of shot peening processes – Part I: studies on 2D interaction laws", *Engineering Computations*, 2000, vol. 17, no. 5, pp. 593–620, DOI: 10.1108/02644400010339798.

[20] E. Oñate, J. Rojek, "Combination of discrete element and finite element methods for dynamic analysis of geomechanics problems", *Computer Methods in Applied Mechanics and Engineering*. 2004, vol. 193, no. 27–29, pp. 3087–3128, DOI: 10.1016/j.cma.2003.12.056.

[21] J. Rojek, *Modelowanie i symulacja komputerowa złożonych zagadnień mechaniki nieliniowej metodami elementów skończonych i dyskretnych*. Warszawa: IPPT PAN, 2007.

[22] M. Lätzel, "From microscopic simulations towards a macroscopic description of granular media", PhD thesis, University of Stuttgart, Stuttgart, 2003.

[23] C. Miehe, J. Schröder, M. Becker, "Computational homogenization analysis in finite elasticity: Material and structural instabilities on the micro- and macro-scales of periodic composites and their interaction", *Computer Methods in Applied Mechanics and Engineering*, 2002, vol. 191, no. 44, pp. 4971–5005, DOI: 10.1016/S0045-7825(02)00391-2.

[24] E. Ramm, G.A. D'Addetta, M. Leukart, "Interrelations between continuum and discontinuum models for geomaterials", presented at VII International Conference on Computational Plasticity COMPLAS, Barcelona, 2003.

[25] S. Nemat–Nasser, M. Hori, *Micromechanics: overall properties of heterogeneous materials*. Amsterdam: North Holland, 1993.

[26] R. Christensen, *Mechanics of composite materials*. New York: John Wiley, 1979.

[27] P. Szklennik, "Identifikacja parametrów modelu numerycznego obudowy tunelowej w gruncie niespoistym", *Biuletyn WAT*, 2018, vol. 67, no. 4, pp. 41–58, DOI: 10.5604/01.3001.0012.8484.

Numeryczne określanie obciążenia modelowej obudowy tunelowej z uwzględnieniem różnych wysokości nadkładu gruntu

Słowa kluczowe: metoda elementów dyskretnych, obudowa walcowa, tunel podziemny

Streszczenie:

W pracy przedstawiono analizę wyznaczania obciążenia modelowej obudowy tunelowej w niespoistym ośrodku gruntowym przy różnych wysokościach nadkładu gruntu nad konstrukcją. W obu przypadkach przeprowadzono szereg symulacji przy konstrukcji obudowy wiotkiej i sztywnej. Analizy dokonano prowadząc symulacje z wykorzystaniem autorskiego programu opartego na metodzie elementów dyskretnych. Wykorzystano model skalibrowany wcześniej na podstawie badań laboratoryjnych. Określono i porównano obciążenia działające na obudowę, rozkład naprężeń w otaczającym ją ośrodku gruntowym oraz przemieszczenia tego ośrodka w otoczeniu konstrukcji. Uwzględniono działanie ciężaru gruntu oraz obciążenia technologicznego zadawanego z powierzchni. Wartości uzyskiwanych numerycznie obciążeń obudowy porównano z obliczonymi według klasycznej metody Hewetta.

Udowodniono, że stopień współpracy między obudową i gruntem jest w obu przypadkach istotnie związany ze sztywnością obudowy, stąd wyznaczone obciążenia mogą znacznie odbiegać od wyników pozyskanych wg klasycznych metod. Wykazano, że na wartość obciążeń przejmowanych przez modelową obudowę istotny wpływ mają jej deformacje oraz górotwór, którego skuteczność uwidacznia się wyraźnie już przy nadkładzie gruntu równym średnicy obudowy i utrzymuje także przy jego większej wysokości. W przypadku konstrukcji wiotkiej redukują się oddziaływania pionowe przekazywane na jej część sklepieniową. Jednocześnie zwiększają się naprężenia pionowe w gruncie w obszarze ociosów wyrobiska, co znacząco intensyfikuje parcie boczne na obudowę. Porównując te wyniki z typowymi schematyzacjami obciążeń w postępowaniach projektowych widać, że schematy te mogą nie ujmować najbardziej niekorzystnej sytuacji obciążeniowej. Różnice mogą dotyczyć zarówno stref bocznych jak i zwornikowej i są widoczne przy mniejszej jak i większej wysokości nadkładu.

Adekwatność modelowania dyskretnego potwierdza ponadto fakt, że umożliwia ono odzwierciedlenie wpływu wysokości nadkładu gruntu na intensywność obciążenia obudowy oraz rozkład naprężeń i przemieszczeń w jej otoczeniu. Przykładem są uzyskane mniejsze oddziaływania poziome w strefach ociosowych przy wyższym nadkładzie. W przypadku przemieszczeń gruntu wykazane są istotne różnice w intensywności osiadań – zdecydowanie większej przy nadkładzie mniejszym. Model dyskretny ujmuje niestacjonarne imperfekcje w ośrodku gruntowym, widoczne w pewnej asymetrii uzyskiwanych oddziaływań. Stosując go uwzględnia się fakt, że grunt ma szkielet wewnętrzny, który podlega interakcji z obudową. Odkształcenia konstrukcji obudowy do wewnątrz wywołują jej odciążenie, natomiast odkształcenia odwrotne, wywołują w gruncie opory bierne, zwiększające całkowite parcie na danym odcinku.